Engineering Geology 343 (2024) 107791

Contents lists available at ScienceDirect

Engineering Geology

journal homepage: www.elsevier.com/locate/enggeo

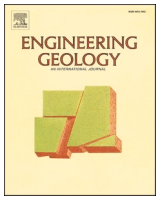

Improving non-uniform gravelly sand using microbially induced carbonate precipitation: An outdoor cubic-meter scale trial by engineering contractors

Guijie Sang [a,b,*], Rebecca J. Lunn [b], Grainne El Mountassir [b], James M. Minto [b], Erica McLachlan [c], David Bradley [c], Kenneth Henderson [c]

[a] Department of Civil and Environmental Engineering, University of Liverpool, Liverpool, UK
[b] Department of Civil and Environmental Engineering, University of Strathclyde, Glasgow, UK
[c] BAM Ritchies, Glasgow Rd, Kilsyth, Glasgow G65 9BL, UK

ARTICLE INFO

Keywords:
Biocementation
Strength improvement
Soil stabilisation
Upscaling MICP
Industrial implementation
Liquefaction resistance

ABSTRACT

Soil improvement using microbially induced carbonate precipitation (MICP) remains largely confined to the laboratory, with only a very small number of large-scale experiments having been completed under field conditions and none by engineering contractors. This study presents a cubic-meter scale improvement of heterogeneous natural sand collected from a local quarry, with a wide variation in grain size, via MICP. The MICP trial was conducted by engineering contractors in a cubic test cell under variable temperatures ranging from 5 °C to 19 °C. The upscaling of cultivation of *Sporosarcina pasteurii* (600 L for each treatment cycle) under non-sterile conditions, as performed by engineering contractors, achieved an optical density (OD_{600}) of 0.89 and a specific urease activity of 2.5 mM urea/min/OD_{600}. Post-MICP-treated sands were subjected to a series of coring, block sampling and laboratory tests. The block sampling process indicated that the majority of sand was effectively cemented, with a small region near a side wall forming a less well-cemented zone, likely induced by less effective fluid delivery in this region. The unconfined compressive strengths of three cores (diameter: 10 cm, length: 22 cm) were 3.6, 4.4, and 7.6 MPa. Consolidated-drained triaxial tests on sub-sampled cores also demonstrated rock-like material behaviour, with a peak friction angle of 43.6° and peak cohesion of 0.64 MPa, and ultimate state frictional angles of 42.0° and ultimate cohesion of 0.12 MPa. The increased shear parameters of the bio-cemented samples (relative to the untreated samples) have many implications for mitigation of geotechnical hazards such as soil liquefaction. The study marks a step forward industrial implementation of MICP for soil improvement by engineering contractors without prior knowledge of MICP.

1. Introduction

Microbially induced carbonate precipitation (MICP) has been proposed for a wide range of geotechnical engineering applications (El Mountassir et al., 2018), including soil stabilisation (Cardoso et al., 2023; Xiao et al., 2022), liquefaction mitigation (DeJong et al., 2022; Montoya and Dejong, 2013), and improvements of erosion and crack resistance (Cheng et al., 2021; Liu et al., 2021, Liu et al., 2020; Salifu et al., 2016; Xiao et al., 2022). Field MICP trials for soil improvement provide crucial information regarding the feasibility, opportunities and challenges of applying this biocementation technique at commercially-relevant scales. Despite the demonstrated success of MICP technology in the laboratory, only a few large-scale outdoor trials in non-sterile, environmentally variable conditions have been reported in the literature (Gomez et al., 2017; Gomez et al., 2015; Miao et al., 2024; Sharma et al., 2022; van Paassen, 2011; van Paassen et al., 2010; Zeng et al., 2021), the majority of which have focused on uniformly or poorly graded soils. A large-scale outdoor MICP trial, on soils with a broad particle size distribution is still lacking. Soil composition, particle shape, and particle size distribution are key factors influencing MICP performance (Ismail et al., 2002), as they directly influence hydraulic flow and solute transport, as well as the physicochemical attachment and physical straining of bacteria (e.g. *Sporosarcina pasteurii*); thus influencing the delivery efficiency and distribution of bacteria and chemicals (Kwak et al., 2023; Sang et al., 2023a; Zamani et al., 2019). The flow, transport, and attachment/straining behaviour of the bacteria in turn determine the precipitation pattern in the treated soil, controlling the effectiveness of bonding at grain-to-grain contact points, the coating on grain

* Corresponding author at: Department of Civil and Environmental Engineering, University of Liverpool, Liverpool, UK.
E-mail address: g.sang@liverpool.ac.uk (G. Sang).

https://doi.org/10.1016/j.enggeo.2024.107791
Received 1 June 2024; Received in revised form 10 September 2024; Accepted 6 November 2024
Available online 9 November 2024

surfaces, and the infilling of pore spaces (Wu et al., 2023), which intrinsically determines the overall cementation efficiency of MICP in the treated soil. Additionally, although in situ geophysical measurements (e.g. shear wave velocity) have been demonstrated as effective monitoring tools in lab-based, large-scale MICP trials conducted on uniform sand (Gomez et al., 2017; van Paassen et al., 2010), no studies have yet investigated their effectiveness in determining the evolution of MICP treatment in non-uniform, heterogeneous soils, where there may be a large variation in grain size and dry density within the initial untreated soil.

Whilst the number of large-scale controlled trials of MICP are increasing, few are conducted in realistic commercial environments. For example, the majority of ureolytically active soil bacteria documented so far exhibit effective urease enzyme production within moderate to high temperature ranges (30–60 °C) with activity increasing as the temperature rises (Steinacher, 2021; Whiffin, 2004). The urease activity at temperatures below 20 °C can be significantly less, making the implementation of MICP in colder climatic zones or seasons challenging. There is still a lack of reported large-scale outdoor MICP trials under low-temperature conditions. In addition, key to achieving a commercial success in MICP field implementation will be training and educating practicing engineers in the fundamentals of the MICP process (Dejong et al., 2013). Despite this, all large-scale field MICP trials reported in the literature have been conducted by researchers with an in-depth knowledge of the biochemical process, and the need to educate and train practising geotechnical engineers with little or no background in microbiology and chemistry to implement MICP, has been largely ignored.

The overall aim and novelty of this study is to assess MICP efficacy of a heterogenous natural sand at large-scale ($1.3m^3$) under varying outdoor temperature conditions between 5 and 19 °C (much lower than most laboratory MICP experiments). This will be done by engineering contractors with no prior experience of MICP, who will be responsible for cultivating and injecting the bacteria and cementing solutions. This study differs from a previous laboratory meter-scale MICP trial (Sang et al., 2023b), as it represents a significant step forward in applying MICP for treating heterogenous natural soil under environmentally variable conditions, whilst tackling one of the greatest challenges in implementing MICP in the field, i.e. to educating and training engineers without background in microbiology, chemistry, and even hydraulics. The trial involved designing and manufacturing a cubic-meter scale test cell, upscaling bacterial cultivation under non-sterile conditions, and conducting MICP treatment cycles using injection protocols previously tested in laboratory meter-scale trials. Core and blocks were sampled from the post-treated sand in the cubic test cell. Subsequently, these samples were subjected to a series of laboratory tests to evaluate the efficacy of the MICP treatment, including unconfined compressive stress tests, X-ray computed tomography (X-CT) scans, P-wave velocity tests, triaxial tests, $CaCO_3$ content tests. This study provides valuable lessons for the industrial implementation of MICP for soil improvement in natural sand deposits.

2. Materials and methods

2.1. Material

The material used in this study was a gravelly sand as delivered from a local quarry in Kilsyth (North Lanarkshire, UK) without any additional processing or treatment (such as autoclaving and washing). The sand consisted of 31.4 % gravel (2–6.3 mm), 64.7 % sand (63 μm - 2 mm), and 3.9 % fines (< 63 μm). The grain size distribution is shown in Supplementary Fig. S1. The median grain size (d_{50}) was 0.75 mm with the uniformity coefficient (C_u) and coefficient of curvature (C_c) being 10.0 and 0.63, respectively, indicating a medium-graded very gravelly sand according to EN ISO 14688-2:2018.

2.2. Bacteria cultivation and urease activity

2.2.1. Upscaled bacteria cultivation under non-sterile conditions

The upscaled cultivation of *S. pasteurii* cells (DSM 33) was conducted by geotechnical engineering contractors under non-sterile condition in two types of reactors (Fig. 1*a&b*): (1) a 1000 L intermediate bulk container (IBC) for MICP cycles 1–5, and (2) two 500 L fermentation vessels for MICP cycles 6–9. The growth media ingredients used in this trial were industrial grade consisting of 5.5 g/L yeast extract, 5 g/L sodium chloride, 0.4 g/L D-glucose, 0.4 g/L di-potassium phosphate, and supplemented with 20 g/L urea. The growth media ingredients, apart from urea, were initially dissolved in boiled tap water, followed by adding tap water and urea to achieve a final temperature of ~30 °C. Subsequently, ~8 % (by volume) bacteria inoculum was inoculated into the prepared media and incubated at 30 °C for 20–24 h. The bacteria inoculum used in the cultivation of bacteria for MICP cycle 1 was grown in a laboratory 50 L fermentation vessel under non-sterile conditions using the type strain DSM No. 33 (DSMZ Culture collection) revived from a fresh frozen −80 °C glycerol stock culture. The same growth media components and concentrations as listed above were used in the fermentation vessels, which were housed in a portacabin onsite. The inoculum used to cultivate the bacteria for MICP cycles 2–4 was taken from the harvested bacteria for MICP cycle 1. After cycle 4, the inoculum for each subsequent cycle (up to cycle 9) was harvested from bacteria from the previous cycle (i.e. cycle 5 bacteria were prepared using inoculum taken from cycle 4, cycle 6 from cycle 5, etc).

Bacterial cultivation in the 1000 L IBC (containing 600 L growth medium) was subjected to agitation using an impeller (diameter: 20 cm, 200 rpm) located at the centre of the IBC (Fig. 1*a*). Two aeration pumps (rate: 960 L/h) bubbled air into the IBC through two porous sandstones, which were located at the bottom of the IBC (one near the southern wall, the other one near the northern wall). The 1000 L IBC was left inside a temperature-controlled warm container (~30 °C) during the daytime and covered with an insulated jacket overnight. Bacterial cultivation in the two 500 L fermentation vessels (each containing 300 L growth medium) was subjected to aeration (aeration rate of each vessel: 960 L/h) from the bottom of the vessels. The vessels were temperature-controlled and set to a constant temperature of 30 °C.

2.2.2. Bacterial density and urease activity

Due to the lack of a spectrophotometer on site, the turbidity (Nephelometric Turbidity Unit or NTU) of the harvested bacteria was measured by engineering contractors on site, and was correlated with bacterial optical density at a wavelength of 600 nm (OD_{600}). The turbidity meter was taken to the microbiological laboratory at the University of Strathclyde and calibrated within the range of 0–900 NTU. Subsequently, the meter was used to determine the turbidity of different bacterial solutions under a range of OD_{600} from 0 to 2.2 (Fig. 2). Bacterial samples (in the stationary phase) were prepared in triplicates to determine their OD_{600} and turbidity. A power law regression was adopted for the estimation of the correlation between bacterial OD_{600} and nephelometric turbidity units as follows: $OD_{600} = 0.01*(NTU)^{0.795}$.

Urease activity of the harvested bacteria was recorded by engineering contractors on site before each injection cycle so as to guarantee effective urea hydrolysis for MICP. The measurement was based on the conductivity method (Whiffin, 2004), i.e., monitoring the changes in electrical conductivity of the mixture of 18 mL 1.11 M urea and 2 mL bacteria suspension over a period of ten minutes. The changes in electrical conductivity (unit: mS/cm) was converted to changes in the urea hydrolysed (unit: mM) using the relationship: urea hydrolysed (mM) = conductivity (mS/cm) * 10.62, as calibrated by Minto et al. (2016). The urease activity is reported is normalised by OD_{600}.

2.3. Preparation of the cubic test cell

Fig. 3 (*a*) shows the outdoor MICP test site at BAM Ritchies in Kilsyth,

Fig. 1. Large-scale cultivation of *S. pasteurii* cells under non-sterile conditions in (*a*) 1000 L intermediate bulk container (IBC) and (*b*) two 500 L fermentation vessels.

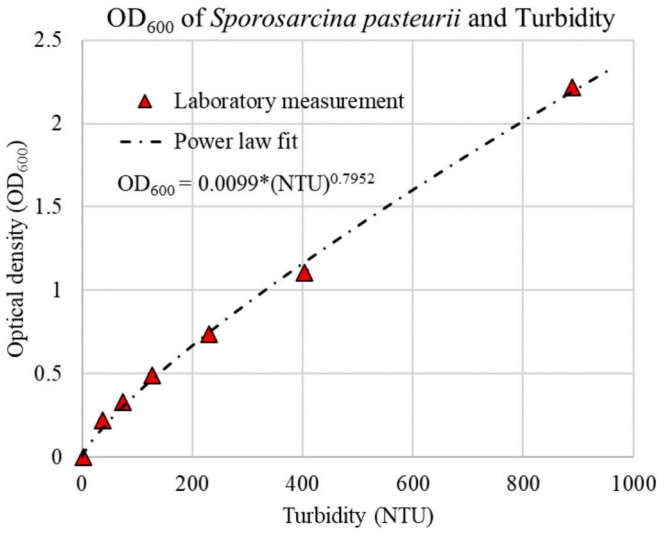

Fig. 2. Relationship between OD_{600} of *S. pasteurii* and nephelometric turbidity. The error bars are too small to be visible.

North Lanarkshire. The test cell was a 1.2 m × 1.2 m × 1.2 m cube with five injections ports installed at the base (Fig. 3*b & c*) which directed fluids horizontally into the cell. The five injection ports were screened with woven mesh (125 μm) and were connected with a hydraulic manifold and an air compressor pump in order to regulate the flow rate. The sand was packed into the test cell to a height of 0.9 m in the following sequence: First, approximately 0.3 m of sand were packed in and then compressed using a 4.5 kg hammer on top of a square sheet of plywood (0.2 m * 0.2 m and 0.018 m thick), lifting the hammer 25 times for each 0.2 m * 0.2 m area of the test cell (total number of hammer blows per layer = 900). Then, the next layer of sand was added, and the process was repeated until a total height of 0.9 m was reached. The final dimensions of the compacted sand was 1.2 m × 1.2 m × 0.9 m (Fig. 3*c*), with 0.3 m of empty space remaining above the sand surface for fluid drainage (Fig. 3*b& c*). A single pore volume (PV) in the cubic test cell was estimated to be 410 L. The top surface of the sand in the cubic cell was covered with perforated sheets to create a free-flowing boundary condition. Prior to the MICP treatment, sand lifting (liquefaction) above the five injection ports was observed during the injection of tap water for the initial saturation process. In response, four 25 kg cement bags were placed on a rack frame above the perforated sheets (Fig. 3*b*) to create a small overburden stress (~0.7 kPa) in order to minimise sand liquefaction near the surface boundary.

2.4. MICP treatment strategy

A two-phase bioaugmentation scheme was applied in the MICP trial, i.e. for each cycle, Phase 1 comprised injection of the bacterial solution; and Phase 2 comprised injection of the cementing solution (i.e. $CaCl_2$ & Urea). Specifically for each treatment cycle (refer to Table 1), 600 L (~1.5 PV) of bacteria solution with an average OD_{600} of 0.89 was first injected, followed by an injection of 2–3 L of tap water for rinsing and cleaning the injection system (i.e. pipelines, inlet ports) followed by a 1-h no-flow period to allow the bacteria to settle and attach. Then in Phase 2, 600 L (~1.5 PV) of cementing solution (0.5 M $CaCl_2$ & Urea) was injected, followed by a 4-h no-flow period. Then an additional 600 L ((~1.5 PV) of cementing solution (0.5 M $CaCl_2$ & Urea) was injected and left with no-flow overnight until the start of the next cycle. The treatment strategy used was based on a similar protocol followed in a previous metre-scale laboratory study by the authors (Sang et al., 2023a, 2023b). After completion of 9 MICP treatment cycles, the test cell was flushed with 2 m^3 of tap water to remove residual chemicals/bacteria. The back pressures and flow rates before MICP treatment, during the 7th MICP treatment cycle, and during the final tap water flush, were recorded for permeability estimation.

2.5. Post-treated core sampling and mechanical testing

The post-MICP-treatment very-gravelly sand was wet cored and subsampled for subsequent mechanical testing in the laboratory.

2.5.1. Unconfined compressive strength (UCS) testing

Three cylindrical samples (diameter: 10 cm; length: 22 cm) cored directly from the cubic test cell were subjected to the UCS test under dry conditions. The top and bottom surfaces of the cylindrical samples were capped with gypsum plaster (Crystacast, compressive strength of 55.2 MPa) to achieve a flat surface, thus avoiding localised stress concentrations during the UCS test. The loading rate was 0.2 mm/min, and the peak axial stress was achieved within ~3–5 min of initiation of loading. The precipitated $CaCO_3$ contents for each specimen at the top, middle, and bottom of the specimens were determined according to ASTM-D4373 (ASTM, 2014). $CaCO_3$ content is reported as the mass of calcite/mass of dry sand.

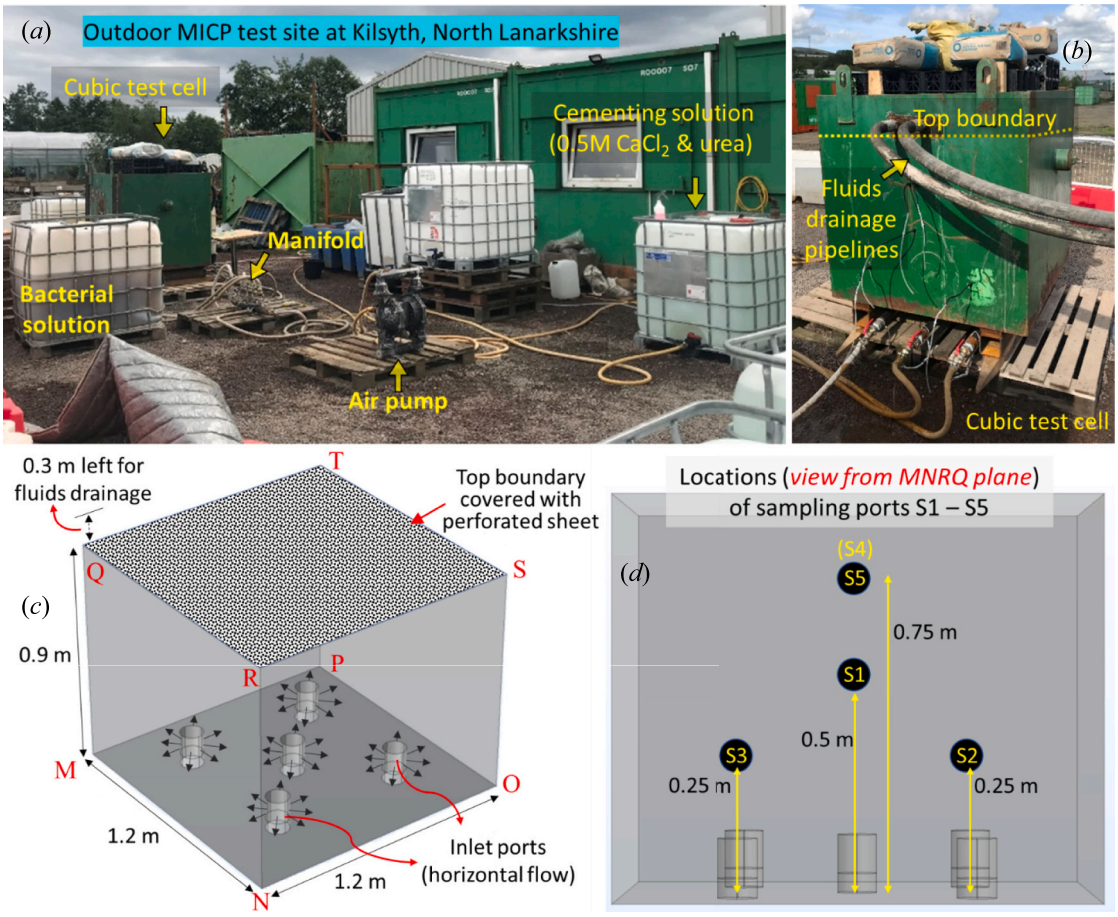

Fig. 3. (*a*) Outdoor MICP test site at Kilsyth, North Lanarkshire, UK; (*b*) side view of the MICP test cell; (*c*) schematic of the soil domain in the test cell (1.2 m × 1.2 m × 0.9 m); (*d*) locations of the five sampling ports.

Table 1
MICP treatment strategy.

Solution type	Concentration	Volume	Flow rate	Duration
Bacteria solution	OD_{600} ~ 0.9	600 L	10 L/min	1 h
Tap water	–	2–3 L	10 L/min	10–20 s
No flow	–	–	–	1 h
Cementing solution	0.5 M	600 L	10 L/min	1 h
No flow	–	–	–	4 h
Cementing solution	0.5 M	600 L	10 L/min	1 h
No flow	–	–	–	Until next cycle

2.5.2. *P-wave velocity testing*

Bulk block samples were removed from the test and subsequently cored. Out of fifty sub-cored cylindrical specimens without clear surface defects (e.g. defects due to large grains plucked from the surface), twenty-two were chosen for P-wave velocity (V_p) determination at a frequency of 54 kHz. These cylindrical specimens (diameter: 5 cm) were trimmed and polished to a length of around 10–11 cm. P-wave velocity for each specimen under dry conditions was determined using a through-transmission method, where acoustic waves were excited at the top surface and received at the bottom. To ensure a good signal-to-noise ratio, two transducer platens were positioned on the top and bottom surfaces of each specimen, applied with coupling gel, and subjected to a constant clamping stress of ~7.5 N (i.e. a load of ~0.75 kg). The P-wave velocity (V_p) was calculated based on the specimen length (L) and the time-of-flight (Δt): $V_p = L / \Delta t$. For comparison, we measured the P-wave velocity of three raw sand samples without MICP treatment under dry conditions. Three untreated sand samples were packed into separate polycarbonate tubes (diameter: 5.2 cm, length: 10.5 cm) using the similar layer packing method. Subsequently, they were oven-dried at 60 °C until no further mass reduction occurred, followed by V_p testing using the same procedure.

2.5.3. *X-ray Computed Tomography (CT) scanning*

Among the twenty-two cylindrical specimens subjected to P-wave velocity testing, four specimens were selected for X-CT scans, using the in-house X-ray CT scanner situated in the Advanced Materials Research Laboratory (ARML) at the University of Strathclyde. The scanning parameters were set to 140 kV, 130 μA, 1415 m-second exposure, 1740 projections, and a 0.25 mm copper filter. The resulting voxel size was 70 μm.

2.5.4. *Consolidated-drained (CD) triaxial testing*

From the twenty-two cylindrical specimens subjected to P-wave velocity testing, eleven were selected for triaxial tests. Among the eleven specimens, nine samples with similar dry densities and P-wave velocities were randomly divided into groups of three samples, and each group was subjected to a different effective confining stress; 100, 300, or 500 kPa. In addition, two other specimens (one with the lowest V_p, one with the highest V_p) were subjected to triaxial CD tests with an effective confining stress of 300 kPa. Each specimen was pre-saturated with de-aired and deionised water under a vacuum for 24 h. After being mounted inside the triaxial cell, the specimens were again flushed with a large volume of de-aired and deionised water to remove any remaining air bubbles. Subsequently, the specimens were back-pressured to achieve a B-value (Skempton, 1954) of 0.95 or higher. The specimens were then allowed to consolidate under the target effective confining pressure

(i.e. 100, 300, or 500 kPa) prior to initiating the drained shearing process. The shearing rate was 0.05 mm/min, until a maximum axial strain of 15 % was reached. The effective confining stress was maintained constant throughout. After triaxial CD testing, the upper, middle, and lower parts of ten specimens were analysed for carbonate content according to ASTM-D4373 (ASTM, 2014).

3. Results and discussion

3.1. Overcoming challenges during the field trial

For each cycle, 600 L of bacterial suspension was prepared on-site under non-sterile conditions. Fig. 4 shows the bacterial OD_{600} and specific urease activity of the bacterial suspension for each of the nine MICP treatment cycles. The average bacteria OD_{600} was 0.89 (standard deviation: 0.18) and the average specific urease activity was 2.5 mM urea/min/OD_{600} (standard deviation: 0.79). Fig. 4 also shows that the bacteria cultivated for the 5th treatment cycle exhibited a noticeable decrease in both urease activity and bacteria OD_{600}. When cultivating bacteria in the 1000 L IBC for treatment cycles 1–5, maintaining a constant temperature of 30 °C was challenging, especially during the overnight period when engineers had to shut off the heating device for safety concerns. To enhance bacteria growth and maintain effective urease activity during the outdoor trial, we recommended that the engineers cultivate bacteria in the two 500 L fermentation tanks that had better temperature control. After changing to the 2 × 500 L fermentation tanks (for MICP cycles 6–9), an increase in bacterial OD_{600} was observed with a fairly constant urease activity between 1.5 and 2.5 mM urea/min/OD_{600}.

During the outdoor trial, the 9 treatment cycles were completed over 25 days from May 30th to June 23rd 2022 due to personnel constraints at the contractors (BAM Ritchies). Fig. 5 marks the onset of the bacterial injection (phase 1) for each treatment cycle (C1 to C9). The outdoor temperature at the trial site location (Kilsyth, North Lanarkshire, UK) during the whole MICP treatment period ranged from 5.0 to 19.0 °C (average: 12.1 °C). In order to be confident that precipitation was occurring over the temperature variations encountered during the field trial, bacteria grown within the University laboratory (from the same group of glycerol stocks) were checked for urease activity and associated calcite precipitation at 4, 10, and 20 °C (refer to Supplementary S2). Our laboratory testing results, as shown in Supplementary S2 – Fig. S2 *a, b & c*, demonstrated that microbially induced carbonate precipitation still occurred for the full range of temperatures encountered during the field trial (i.e. 5–19 °C), although the precipitation rate was slower at lower temperatures. Note that the injection activity and early-stage reaction of bacteria and cementing solution occurred during the daytime (09:00–21:00), with the average temperature ranging from 10.4 to 18.8 °C (average: 14.2 °C).

Throughout the MICP treatment cycles, only a small back pressure increase occurred whilst maintaining the same pumping rate for each fluid injection (i.e. 10 L/min). This implies that no significant permeability decrease occurred as a result of calcite precipitation. Permeabilities of the sand in the cubic cell were calculated based on injection rate and pressure recorded prior to treatment, during the 7th MICP cycle, and after the 9th MICP cycle; these were estimated to be 3.5×10^{-12}, 1.9×10^{-12}, and 1.4×10^{-12} m^2, respectively. Therefore, over the course of nine MICP treatment cycles there was a slight decrease in permeability due to MICP treatment.

3.2. Post-treatment core recovery and block sampling

After MICP treatment, the eastern wall (boundary OPTS in Fig. 6*a*) and overburden (four 25 kg cement bags) were removed. A thick layer of calcium carbonate was observed on the top boundary due to settlement of bacteria within the fluid present above the sand during MICP treatment. After removing the calcium carbonate layer, as well as the perforated sheets, cores were drilled from the top face (Fig. 6*b*). Initial coring attempts used a core barrel with an inner diameter of 5 cm, this resulted in significant challenges for the on-site contractors; the barrel was prone to jamming at depths of around 15–20 cm and usable cores could not be recovered. As a consequence, a larger core barrel (inner diameter: 10 cm), which was more powerful was deployed. The 10 cm (in diameter) coring results are shown in Supplementary S3 Fig. S3. The more powerful coring bit enabled some cores to be drilled with core recoveries of between 0 m and 0.9 m into the cubic test cell. As has been reported elsewhere, even with the larger core barrel, drilling intact cores from the biocemented gravelly sand in situ posed a challenge (Sang et al., 2023b; van Paassen, 2011) due to: (1) local stress concentrations caused by the coring bit hitting large irregular gravel particles, which then rotate and fracture the core, (2) hydraulic disturbance from the drilling fluid that sometimes eroded the biocemented sand, and (3) an unstable coring frame which caused vibration of the barrel during coring. Following in situ coring, large blocks of the biocemented gravelly sand were saw cut and chiselled from the test cell (Supplementary S4 –

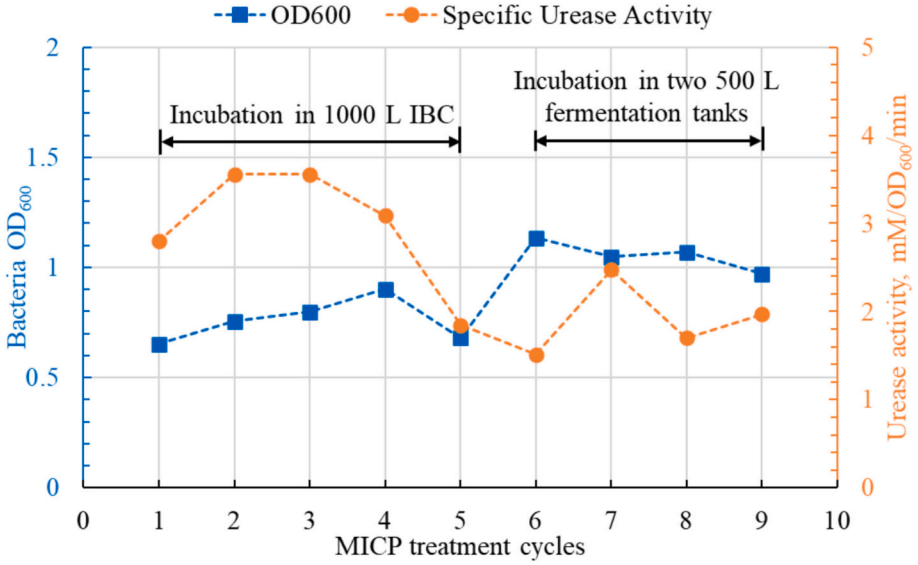

Fig. 4. Bacterial OD_{600} and specific urease activity (measured right after bacterial harvesting) for MICP cycles.

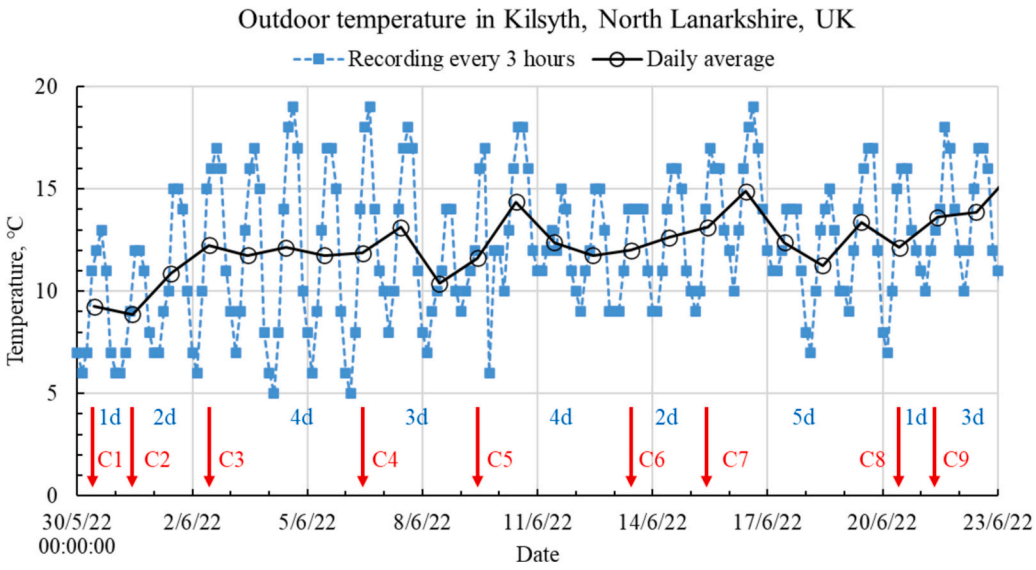

Fig. 5. Outdoor temperature in Kilsyth, North Lanarkshire, UK. Data obtained from web page (World Weather Online, 2022). Red arrow marks the start of the injection of bacterial solution for each cycle (e.g. C1 means cycle 1). Duration of each cycle was marked in blue font. (For interpretation of the references to colour in this figure legend, the reader is referred to the web version of this article.)

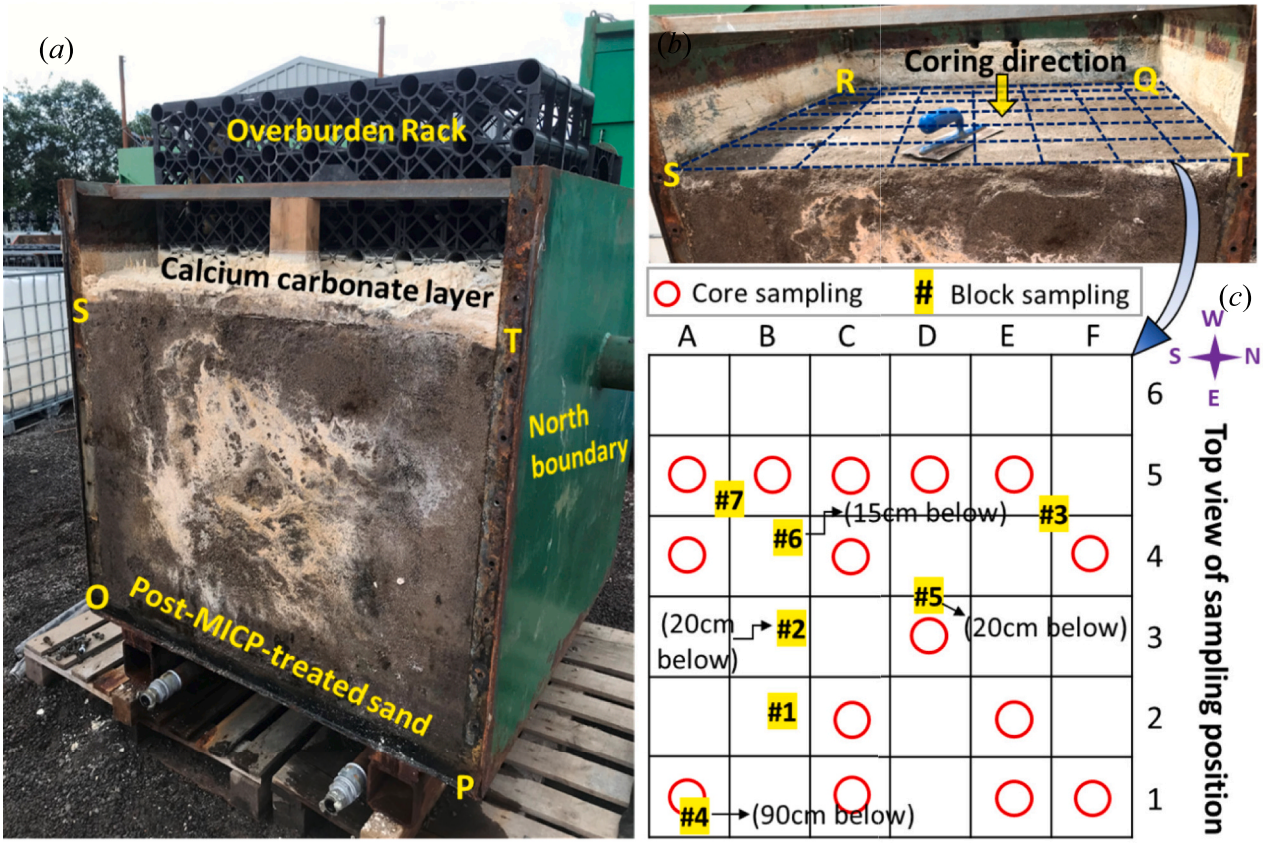

Fig. 6. (*a*) MICP test cell after 9 cycles of MICP treatment after removing the east wall. (*b*) an image of the treated very gravelly sand after removing the overburden and the top sheet. (*c*) top view of the sampling position; red circle marks the positions where 10-cm cores were sampled; #1-#7 marks the positions where blocks were sampled, with texts describing the sampling depth if they were not sampled from top surface. (For interpretation of the references to colour in this figure legend, the reader is referred to the web version of this article.)

Fig. S4*a*). Some of these sampled blocks underwent a sub-coring process (diameter: 5 cm) in the geomechanics laboratory at the University of Strathclyde, utilising a more stable control frame (Supplementary S4 – Fig. S4*b*). The locations of the 10-cm cores, and the blocks from which sub-cores were sampled, are marked in Fig. 6*c*.

Fig. 7*a* shows the top view of the MICP-treated sand after the coring process. The remaining well-cemented zones where solid blocks could be sampled are delineated by the yellow solid line. The zone on the left-

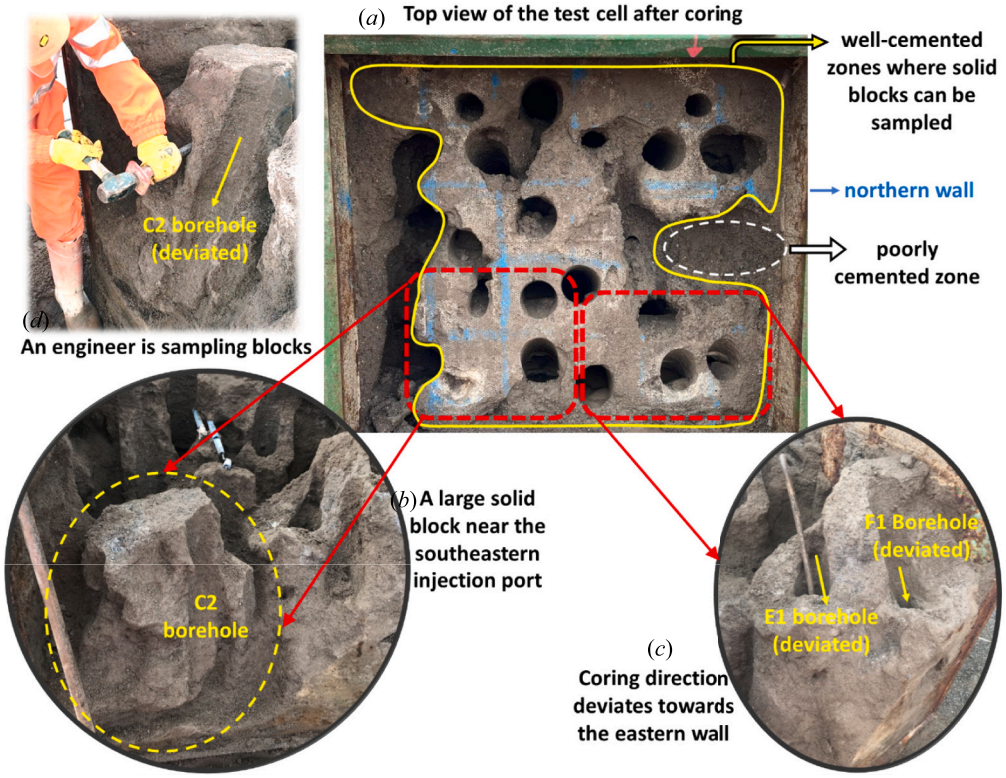

Fig. 7. (*a*) Top view of the test cell after coring showing well-cemented zones where solid blocks were sampled; (*b*) close-up image of a large solid block near the southeastern injection port; (*c*) two core runs (E1 & F1) deviating toward the eastern wall; (*d*) block sampling by an engineer.

hand side of the Figure was severely damaged by the unsuccessful coring activity so the properties after treatment are not documented. A large solid block near the southeastern injection port, as depicted in the close-up image marked by the yellow dashed circle in Fig. 7*b*, presented significant challenges for the engineering contractors attempting to chisel it out of the cubic cell (Fig. 7*d*). The average $CaCO_3$ content at the top part of this large block (Fig. 7*b*) was determined to be ~0.175 (standard deviation: 0.031), as estimated from the $CaCO_3$ content of eight 50 mm cylindrical specimens sub-cored in the laboratory from the top of the block (each specimen was tested for $CaCO_3$ content three times, near the top, middle and bottom). This high concentration of $CaCO_3$ cementation is likely attributed to preferential flow paths in this region which is located above an injection port, allowing for preferential delivery of bacteria and cementing solutions. Indeed, during the 4th cycle of MICP treatment, sand liquefaction above the southeastern injection port was observed. To prevent this, the injection rate through the southeastern port was reduced by approximately 50 % after cycle 4, by adjusting the hydraulic manifold for the remaining cycles. During block sampling, high levels of cementation were also observed in the northeastern part of the cubic cell, where core runs E1 and F1 deviated toward the eastern wall around highly cemented zones (Fig. 7*c*). The cell contained one poorly-cemented region (Fig. 7*a*), between the two injection ports near the northern wall, as marked by the white dashed line in Fig. 7*a*.

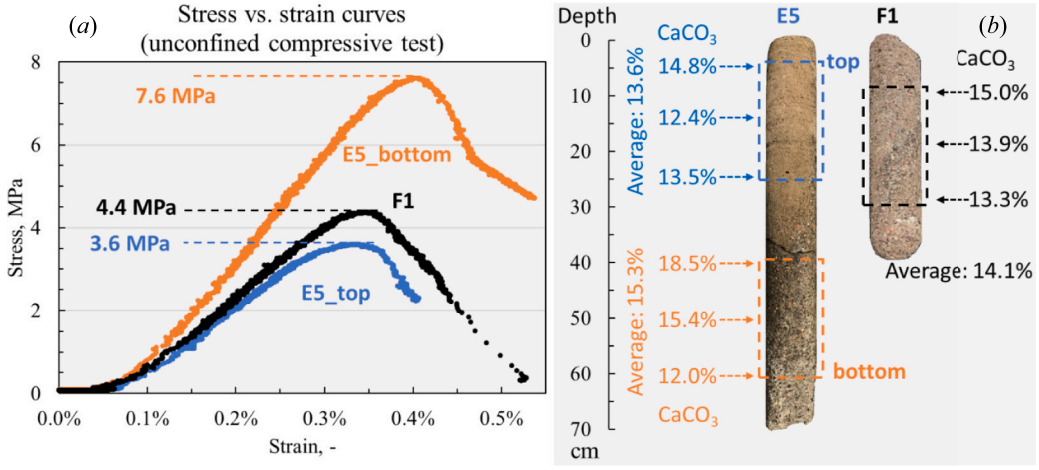

Fig. 8. (*a*) Stress-strain curves of the three 10-cm cores (two cut from core run E5 and one from F1) during UCS test; (*b*) images showing the cutting positions of the specimens and their $CaCO_3$ contents.

3.3. Unconfined compressive strength (UCS) test

Fig. 8*a* shows the stress-strain curves from unconfined compressive tests for three of the cores (diameter: 10 cm; length: 22 cm) located in Fig. 6*c*. Specimen F1 was cut from core run F1 (marked by the black dashed rectangle in Fig. 8*b*); specimens E5_top and E5_bottom were cut near the top and bottom of core run E5, as marked by the blue and orange dashed rectangles in Fig. 8*b*. Visual inspection of the photograph in Fig. 8*b* shows that the E5_top appears to be comprised of increasing more finer material from the bottom to the top (close-up images are available in Supplementary S5 - Fig. S5). This is likely caused by soil separation during the initial soil lifting above the injection port (prior to the MICP treatment), which resulted in soil resettlement with more coarser materials (gravels) settling at the bottom while finer grains settling at the top. The UCS values were 3.6 MPa, 7.6 MPa, and 4.4 MPa for cores E5_top, E5_bottom, and F1, respectively; their corresponding Young's moduli were 1.7 GPa, 2.5 GPa, and 1.8 GPa, as derived from the slope of the linear portion of the stress-strain relationship. The average $CaCO_3$ contents for the three specimens were 13.6 % for E5_Top, 15.3 % for E5_Bottom, and 14.1 % for F1 (Fig. 8*b*). Among the three specimens, a higher $CaCO_3$ content, indicative of increased carbonate precipitation, corresponded to higher UCS and Young's modulus values. Note that even with similar $CaCO_3$ content, the UCS values of the bio-cemented granular soil are highly dependent on grain size and shape, the uniformity of $CaCO_3$ precipitation, as well as the presence of fines (Ma et al., 2022; Ma et al., 2021). In this study, the non-uniformity distribution of soil gradation along the depth, due to packing process and initial soil lifting, could cause variations in UCS among the three drilled specimens. Further, specimen E5_Bottom experienced a shear failure at the base of the core, as depicted in Supplementary S6 - Fig. S6*b*, where the $CaCO_3$ content was lower (12.0 %). Whereas, specimen F1 exhibited a distinct shear band, as seen in Supplementary S6 - Fig. S6*c*. To summarize, the post-treatment mechanical behaviours of the three cylindrical specimens resembled that of rock-like materials, with unconfined compressive strengths ranging from 3.6 to 7.6 MPa.

3.4. Consolidated-drained (CD) triaxial test results

V_p and dry density were determined for all of the 5 cm sub-sampled cores and used to select nine cores for triaxial testing with similar dry densities and P-wave velocities (supplementary S7 Fig. S7); thus ensuring they were as close to replicates as possible. To better understand the role of P-wave velocity, we also tested (CD triaxial) the core exhibiting the highest V_p and the core exhibiting the lowest V_p (Fig. S7). Triaxial test results for the nine bio-cemented specimens with a similar V_p are shown in Figs. 10, 3 specimens were tested at each effective confining stress level of 100, 300 and 500 kPa. The response of 3 untreated sand specimens is also shown in Fig. 10 for comparison. The MICP-treated specimens exhibited a brittle behaviour, with peak deviatoric stress (failure) achieved at an axial strain ranging from 1.0 % to 1.6 % (Fig. 9*a*). Post-peak the specimens exhibited strain softening behaviour with a rapid decline in deviatoric stress within an axial strain range of 1.6 % to 3.0 %, followed by a gradual reduction until reaching a constant value representing the ultimate shear strength. The peak deviatoric stresses (Fig. 9*a*) were in the range of 3.3–4.2 MPa at an effective confining stress of 100 kPa; 4.1–4.8 MPa at 300 kPa; and 4.2–5.7 at 500 kPa. The average ultimate strengths were approximately 1.0, 1.8, and 2.4 MPa at confining stresses of 100, 300 and 500 kPa respectively. As expected, higher effective confining stresses corresponded to higher peak deviatoric stresses and ultimate shear strengths as a result of higher frictional forces. These observations are consistent with conventional soil behaviour and have previously been observed for MICP treated sands as reported by Feng and Montoya (2016), Nafisi et al. (2020), and Wu et al. (2021). Compared to the three untreated samples (solid lines in Fig. 9 *a*), the nine MICP treated cores (dashed lines in Fig. 9 *a*) exhibited higher peak deviatoric strength and higher ultimate strength, Note that three of the CD triaxial tests were terminated prior to reaching an axial strain of 15 % due to leakage of the specimen membrane, which most likely occurred due to the presence of angular shaped, sharp-edged gravels.

Fig. 9*b* presents the corresponding volumetric strain behaviour during the CD tests for the same nine MICP treated cores and the three untreated samples under the three effective confining stresses. In this study, we adopt the convention that positive values denote contraction. As deviatoric stress increased, the tested specimens initially underwent a phase of contraction followed by dilation. The peak contraction, indicative of the densest state, was observed at axial strains ranging from 1.0 % to 1.4 %, slightly before the axial strains at which the deviatoric stress reached its maximum value. After the peak contraction phase, the bio-cemented specimens commenced dilation, attributed to the rolling and sliding of particles and the fracturing of cementing bonds that accompanies the brittle failure (as characterised by a sharp drop in deviatoric stress). As expected, as the confining stress increased the volumetric behaviour becomes less dilative. These observations align with a study

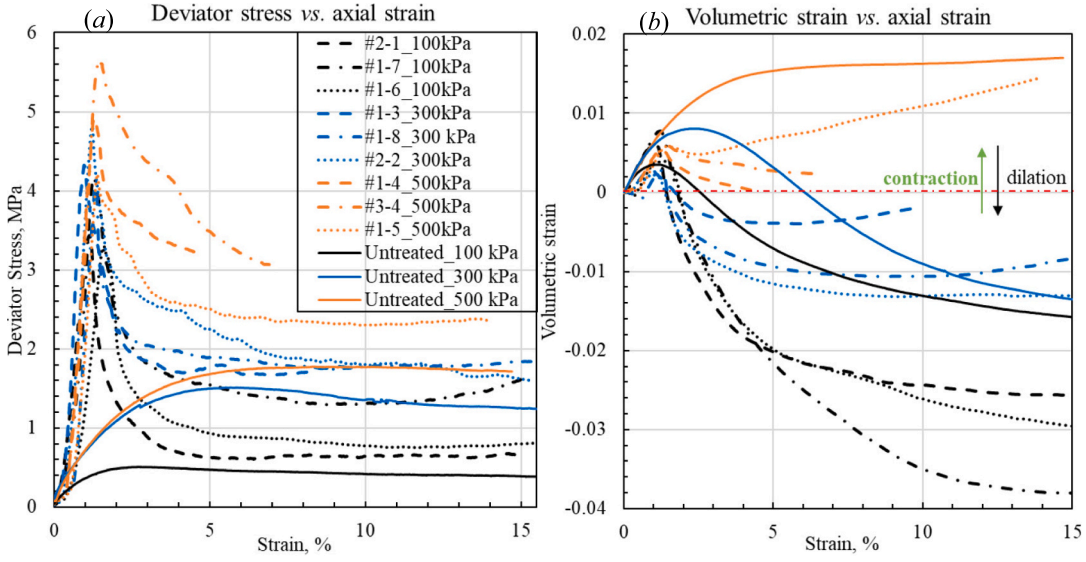

Fig. 9. CD triaxial test results under three effective confining stress (100, 300, 500 kPa). (*a*) deviatoric stress plotted against axial strain; (*b*) volumetric strain plotted against axial strain.

by Clough et al. (1981) who conducted drained triaxial tests on cemented sands and found that strong dilation occurred at lower confining stress levels and diminished as the confining stress increased. Feng and Montoya (2016), Alshibli and Cil (2018), and Nafisi et al. (2020) have also observed reduced dilative behaviour of MICP cemented sands with increasing effective confining stress. Compared to the three untreated samples (solid lines in Fig. 9 *a*), the MICP treated cores (dashed lines in Fig. 9 *a*) exhibited higher dilatancy under the same effective confining stress.

Fig. 10 shows the CD triaxial results for two specimens (selected from the 5 cm diameter sub-cores) that had the lowest and highest P-wave velocities (Fig. S7, supplementary information). Both samples were tested under an effective confining stress of 300 kPa. For comparison, the results for the three specimens in Fig. 9 (i.e. #1–3, #1–8, #2–2) tested under a confining stress of 300 kPa are also presented in Fig. 10. As anticipated, specimen #1–10 with the lowest P-wave velocity (V_p) and dry density had the lowest peak deviatoric stress (3.7 MPa), whilst specimen #5 with the highest V_p and dry density had the highest peak deviatoric stress (5.9 MPa). In terms of volumetric strain, specimen #5 with the highest V_p had the highest dilation (3.5 %) of all the specimens at a confining stress of 300 kPa, whilst the remaining samples exhibited similar behaviour.

Fig. 11 (*a*) and (*b*) shows the peak and critical state strengths against the mean effective stress *p*' (and the stress paths followed) for the bio-cemented sand for all eleven samples in Fig. 9 and Fig. 10, plus the 3 untreated specimens. The deviatoric stress *q* and mean effective stress *p*' are defined as $q = \sigma_1\text{-}\sigma_3$ and $p' = (\sigma'_1 + 2\sigma'_3)/3$, in which σ'_1 is the axial stress minus the pore water pressure and σ'_3 the effective confining stress respectively. Note the friction angle was determined knowing that the slope of the line in *q-p'* space is equal to $\frac{6Sin\phi'}{3-Sin\phi'}$ and the y-intercept is equal to $\frac{6c'Cos\phi'}{3-Sin\phi'}$. Based on the peak strength failure envelope of the nine grouped MICP-treated specimens (Fig. 11*a*), the peak cohesion and peak frictional angle were determined to be 0.64 MPa and 43.6°, respectively. These values were higher than the cohesion (0 MPa) and peak frictional angle of the untreated sand (42.3°), as determined from the failure envelope of the untreated sand in Fig. 11 (*a*). Based on the failure envelopes at critical state (Fig. 11*b*), the ultimate frictional angle for the MICP-treated sand was determined to be 42.0°, which is also higher than that for the untreated sand (40.7°). This increase in peak and ultimate frictional angle due to MICP treatment has also been observed by Feng and Montoya (2016) and Nafisi et al. (2020), who studied uniformly-graded sand with laboratory centimetre-scale MICP treatment. The increase in peak and ultimate frictional angles of medium-graded very gravelly sand, resulting from large-scale MICP treatments, hasn't been previously reported. Interestingly, the ultimate cohesion of the MICP-treated sand at critical state was determined to be 0.12 MPa, which is 18.8 % of the peak cohesion. Zhang and Dieudonné (2023) simulated the effect of four distribution patterns of precipitated $CaCO_3$ on the mechanical behaviour of bio-cemented sands, i.e. contact cementing, bridging, grain coating, and pore filling. They found that the ultimate cohesion was 7.7 kPa at 3 % $CaCO_3$ content for the bridging pattern, which is also 18.0 % of the peak cohesion (42.8 kPa). The ultimate cohesion of bio-cemented sand is possibly a result of unbroken bond near the shear band zone (Zhang and Dieudonné, 2023).

3.5. Correlation between P-wave velocity and $CaCO_3$ content

Fig. 12 shows $CaCO_3$ content plotted against P-wave velocity (V_p) for the eleven triaxial specimens and the three untreated 'control' sand specimens (Fig. 12*a*). The MICP-treated cores exhibited V_p ranging from 2073 m/s to 2496 m/s, and $CaCO_3$ contents ranging from 0.137 to 0.204. In contrast, the three untreated sand specimens, exhibited P-wave velocities in the range of 286–363 m/s, and zero $CaCO_3$ content. In most studies (Gomez et al., 2017; van Paassen et al., 2010), the monitoring of S-wave (shear) and/or P-wave (compressive) velocities has been shown to be an effective indicator of bio-cementation, with strong positive correlation demonstrated between $CaCO_3$ content, S-/P- wave velocity, and soil strength (Weil et al., 2012). In this study, we observe a clear increase of approximately one order of magnitude in V_p (Fig. 12*a*) from untreated sands to MICP treated sands. However, there is no correlation (Fig. 12*b*) between the small range of $CaCO_3$ content in the subsampled cores (0.137–0.204) and their respective P-wave velocities. No correlations were observed either between peak and ultimate strengths, secant modulus, and $CaCO_3$ content (refer to Supplementary S8 Fig. S8). To investigate this lack of correlation between small variations in $CaCO_3$ content after treatment and V_p, X-CT scans were conducted on four of the triaxial cores (Fig. 13). Two pairs were selected to have similar $CaCO_3$ content but with very different values of V_p (samples identified in Fig. 12*b*), #1–7 and #5 with calcite content between 0.15 and 0.159 and #2–1 and #1–6 with calcite content between 0.182 and 0.185. Visual inspection of the X-CT scans (Fig. 13) shows that the initial granular material and the subsequent $CaCO_3$ precipitation is highly heterogeneous within the cores, with patches of finer grained sand, regions with larger grains and visibly higher porosity, and highly cemented regions with little visible pore space. Comparing #1–7 and #5, we can see that

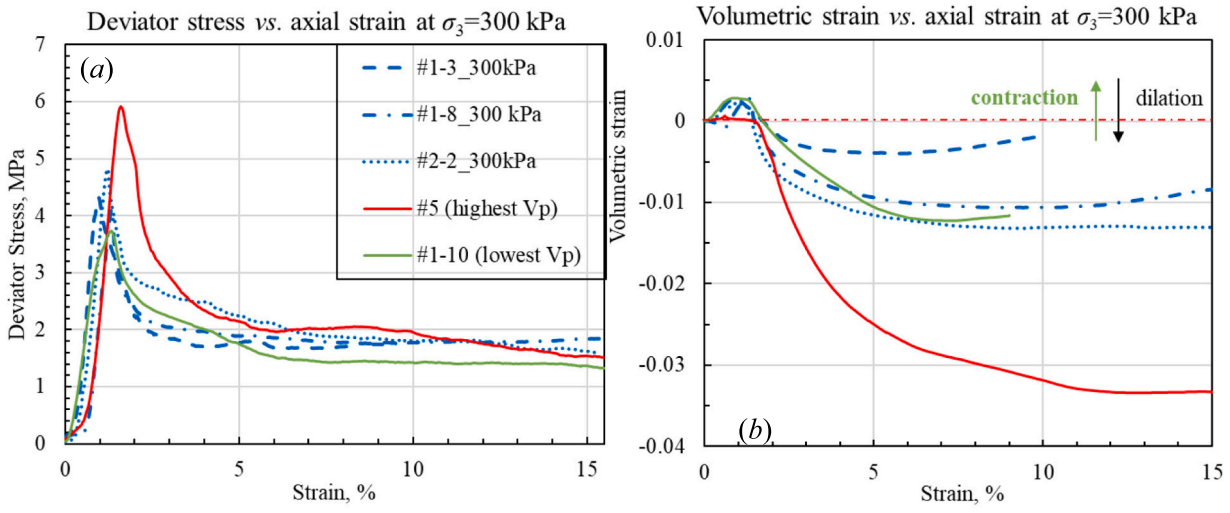

Fig. 10. CD triaxial test result under an effective confining stress of 300 kPa. (*a*) deviatoric stress plotted against axial strain; (*b*) volumetric strain plotted against axial strain.

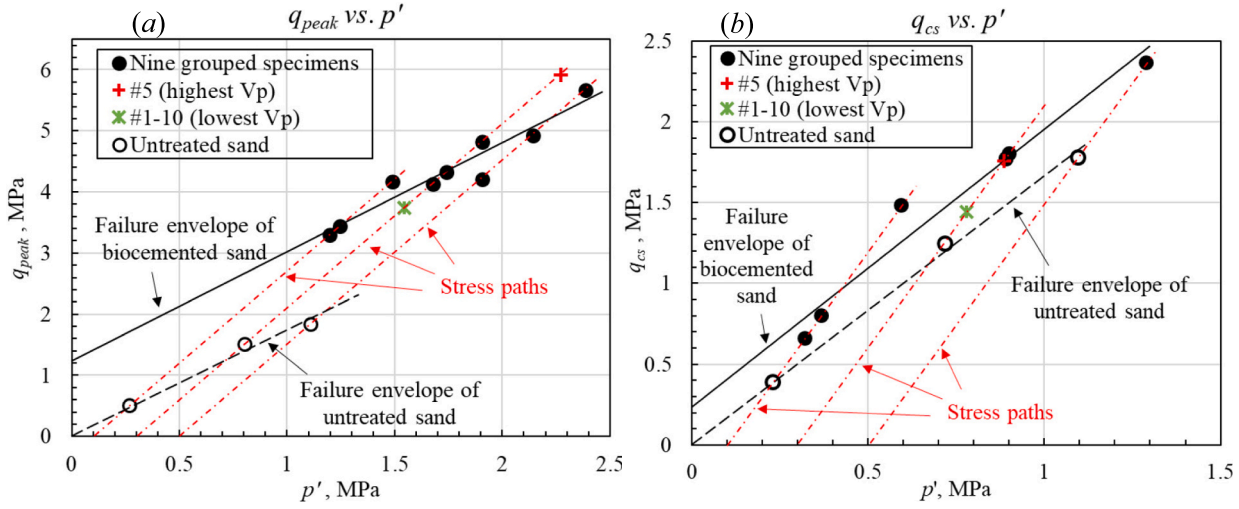

Fig. 11. (*a*) peak strength and (*b*) ultimate strength at critical state of the treated specimens and untreated sand against the corresponding mean effective stress *p*'.

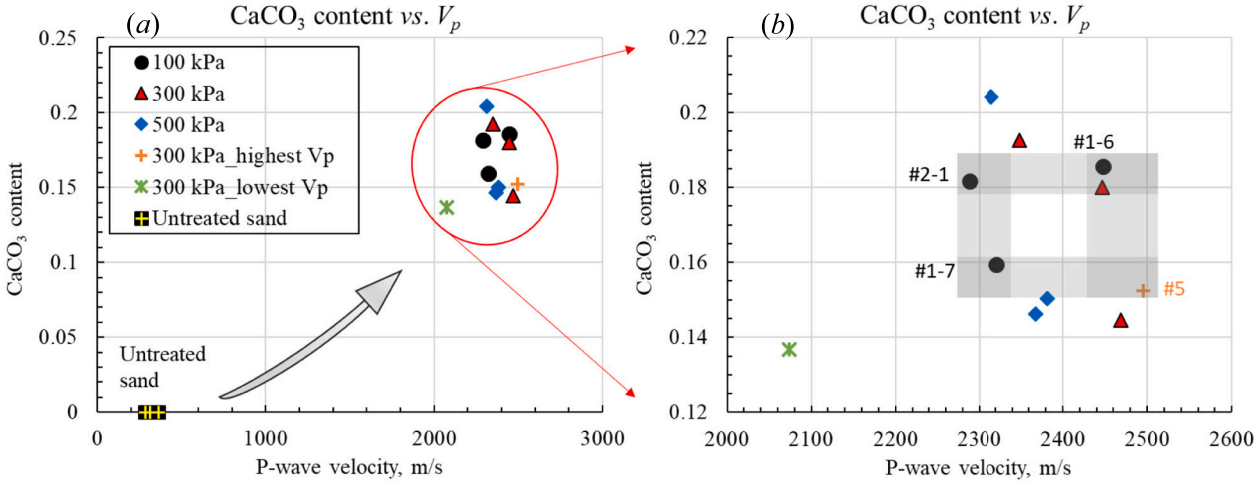

Fig. 12. (*a*) $CaCO_3$ content plotted against V_p for the eleven sub-sampled cores subjected to the triaxial test and for the three untreated sand samples (untreated); (*b*) zoomed-in plot with the four X-CT scanned samples labelled.

#1–7 comprises considerably more large gravel particles and subsequently has a more porous structure, whereas #5 contains more finer-grained particles with very few visible large pores (consistent with its higher dry density). #1–7 has a much lower V_p, (2321 m/s) and #5 has a much higher V_p, (2496 m/s). Given that both cores have a similar calcite content (0.15–0.159), the difference in V_p is attributed to the very different initial microstructure of these cores pre-MICP treatment; for cores with larger grain sizes and higher porosity there are fewer contact points for wave transmission. Despite the difference in their $CaCO_3$ contents Core #2–1 has a similarly low value of V_p to #1–7; visual inspection of the X-CT scan shows #2–1 is characterised by gravel-sized particles with high porosity regions. Whereas Core #1–6 with similar calcite content to #2–1, exhibits a V_p value similar to #5. Core #1–6 has a lower dry density but higher $CaCO_3$ content than #5, suggesting that this core started with a more porous structure than Core #5 and the high calcite content (0.185) is responsible for reaching a high V_p value (similar to Core #5), indeed the X-CT scan shows a very well cemented region toward the bottom right hand side of the core which may account for the high V_p measured. In general, Fig. 13 indicates that small-scale variations in V_p between treated cores are governed by a combination of the initial dry density, the spatial variations in porosity and local spatial variations in grain sizes as well as the $CaCO_3$ content achieved, all of which alter the density of cemented contact points between grains.

The variability in grain size and distribution during the sand packing process directly influences the dry density and P-wave velocity of different regions within the medium-graded gravelly sand, as well as causing local variations in delivery of the bacteria and cementing solutions during treatment (due to variations in permeability and porosity) and thus in the $CaCO_3$ distribution. Since all natural soil deposits will exhibit prior spatial variation in grain size, shape and spatial distribution, it will be crucial to conduct in situ monitoring of seismic wave velocity both prior to, and after, MICP treatment so that changes in V_p (or S-wave velocity) can be used to estimate local $CaCO_3$ content, rather than relying on the absolute values for evaluating the uniformity of MICP treatment.

4. Implications for Field Implementation of MICP in Engineering Geology

4.1. Field implementation of MICP for heterogeneous soil: Progress and limitations

This is the first pilot study of the large-scale implementation of MICP for the improvement of heterogenous natural soil carried out by

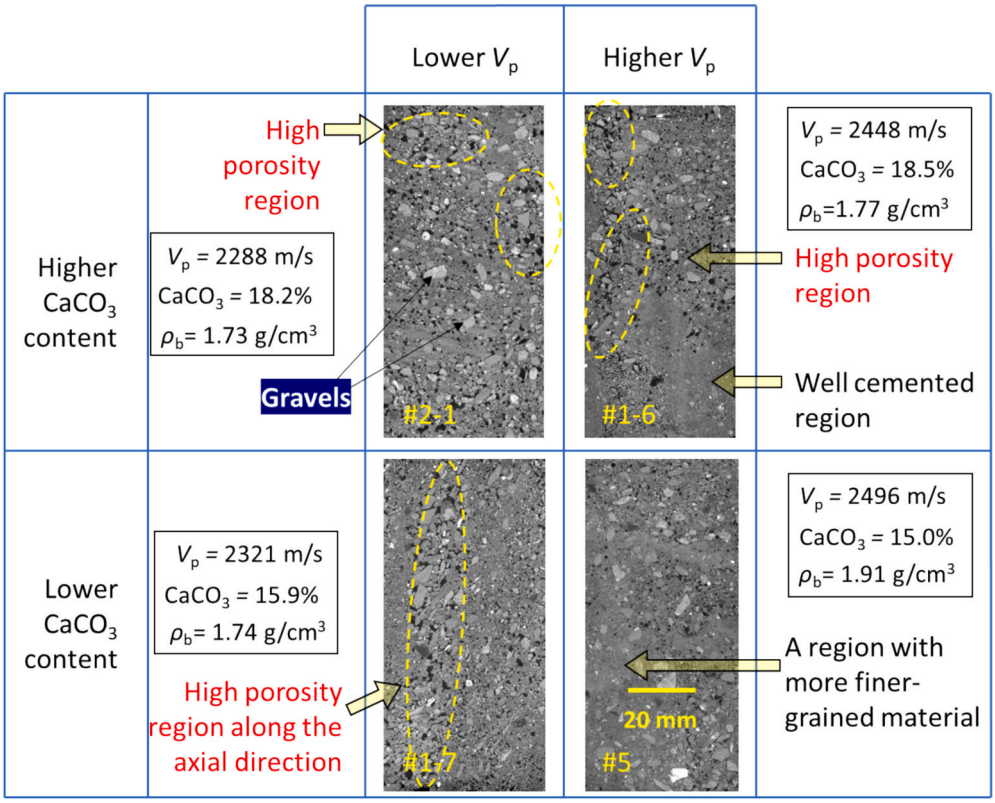

Fig. 13. X-CT images of the four sub-cored specimens (identified in Fig. 12*b*) grouped in similar $CaCO_3$ content and V_p. Note that V_p was measured in the axial direction.

engineering contractors with no prior knowledge of the MICP process. In this study, the injection strategy of MICP for the cubic test cell was derived from a previously tested laboratory trial involving meter-scale experiments in a radial flow cell (Sang et al., 2023b). After undergoing relevant technical training, risk assessments and safety training in bacterial cultivation and handling, the engineering contractors successfully treated natural soils at the cubic-meter scale. This was accomplished outdoors where bacterial urease activities could be inhibited by low temperatures that ranged from 5 to 19 °C (average: 12.1 °C). This study has demonstrated that a usable bacteria density (~0.89 OD_{600}) and urease activity (2.5 mM/min/OD_{600}) can be achieved within upscaled bacterial cultures (600 L) cultivated by engineering contractors under non-sterile environmental conditions utilising industrial-grade ingredients (i.e. yeast extract, urea, and other chemicals). A recent work by Omoregie et al. (2020) demonstrated the successful utilization of a custom-built steel reactor (3 m^3) to scale up *S. pasteurii* culture production within a non-sterile environment, employing food-grade medium ingredients. Nevertheless, there still remains a need for additional effort to optimise the process (Chen et al., 2022; Omoregie et al., 2017), as well as to develop large-scale bacterial storage methodologies accessible to the engineering industry. Such efforts are crucial for achieving commercial success in the context of MICP applications. Several cost-effective measures can be implemented to further enhance bacterial production. These measures include elevating the dissolved oxygen levels within cultures by increasing aeration and agitation rates, and storing bacteria during their exponential/stationary phase within a cold room for future use as inoculants.

This study has several limitations that must be addressed to achieve cost-effective and sustainable field implementation of MICP. For example, the study focused on training engineering contractors to deliver viable MICP improvements to heterogeneous natural soils in the field. A two-phase bioaugmentation method—injecting bacterial solution in each of the nine cycles—was used, potentially leading to incomplete bacterial utilization and unnecessary costs. Gomez et al. (2017) demonstrated similar cementation improvements in poorly-graded sand (meter-scale) by stimulating indigenous bacterial species. Lee et al. (2023) also demonstrated a relatively uniform cementation in sand columns based on bio-stimulation. However, the effectiveness of biostimulation is highly site-specific, requiring the stimulation of native ureolytic species with suitable nutrients under favorable conditions (e.g., pH, temperature, oxygen levels), which can be time-consuming for enough bacterial population growth. A combination of bioaugmentation and biostimulation, such as injecting bacterial solution in the first cycle followed by several cycles of biostimulation, could be a cost-effective yet underexplored approach. Additionally, due to staff work-hour constraints, the static time for bacterial attachment and the reaction time for the first cementing solution were set at 1 h and 4 h, respectively. These times could be extended, depending on factors such as the calcium conversion rate observed in laboratory batch experiments, to enhance bacterial attachment and calcium conversion efficiency, thereby reducing material costs. Another limitation of this trial is the absence of ammonium removal, which poses an environmental risk to the surrounding soils or groundwater if left untreated. Developing scalable methods for monitoring, remediating or eliminating ammonium by-products following bio-cementation remains needed (Rodríguez and Cardoso, 2024).

4.2. Implications in engineering geology

The improvement of mechanical properties of MICP-treated heterogeneous natural soils through in situ bio-grouting has many implications for mitigation of geological and geotechnical hazards such as soil liquefaction, as triggered by the loss of soil strength due to an increase in pore water pressure during static or dynamic loads (e.g. earthquakes). Our large-scale MICP trial shows an enhanced unconfined compressive strength (up to 7.6 MPa) and shear parameters, such as bio-cementation

induced cohesion (from 0 to 0.64 MPa) and peak frictional angle (from 42.3° to 43.6°), without inducing much permeability reduction (3.5–1.4 $\times 10^{-12}$ m^2). The improvement of soil strength will increase the bearing capacity of geotechnical structures such as foundations, mine tailing slopes, and embankment, thus enhancing their liquefaction resistance to seismic response, as also demonstrated by small-scale centrifuge model tests (Darby et al., 2019; Montoya et al., 2013; San Pablo et al., 2024) and seismic shake table tests (Zhang et al., 2020). In the meantime, the remaining high soil permeability after MICP treatment allows pore water to be dissipated freely without inducing too much excess pore pressure after the cementation degrades during earthquake loading. Furthermore, the bio-cementation induced an increase in the ultimate frictional angle from 40.7° to 42.0°, which further enhance the liquefaction resistance even after the loss of cementation bonds under seismic loads. Although all these improved shear parameters positively impact on the mitigation of soil liquefaction through biocementation, it remains an open question how the extent and uniformity of biocementation will influence the liquefaction resistance of heterogenous soil on a large scale under seismic loads. Overall, the study provides valuable insights into the practical challenges and opportunities associated with upscaling MICP for commercial use, paving the way for more widespread adoption of this innovative soil stabilisation technology in engineering geology.

5. Conclusion

A successful cubic-meter scale MICP trial on as-delivered gravelly sand was conducted by engineering contractors in outdoor (5–19 °C) conditions. This included large-scale cultivation of ureolytic bacteria (*S. pasteurii*) under non-sterile conditions in the field, performing nine MICP treatment cycles over 25 days, and post-treatment core and block sampling after the MICP treatment. The treatment efficacy was assessed through a series of geo-mechanical and microstructural analyses on the core/block samples, including unconfined compressive strength tests, P-wave velocity tests, consolidated-drained triaxial tests, X-CT scans, and flow simulations. The main conclusions are summarised below.

Upscaled bacterial cultivation under field non-sterile conditions achieved an average bacteria OD_{600} of ~0.89 and a specific urease activity of ~2.5 mM urea/min/OD_{600}. During the trial, the outdoor temperature ranged from 5 to 19 °C. Laboratory batch experiments conducted in parallel demonstrated that although the specific urease activity of *S. pasteurii* was significantly higher at higher temperatures (0.66, 1.5 and 2.1 mM/min/OD_{600} at temperatures of 4, 10 and 20 °C respectively), Ca^{2+} conversion rates of 72.2 %–88 % were still achieved at temperatures between 4 and 10 °C within the first 20 h. This provided direct evidence that carbonate precipitation was occurring within the test cell throughout, despite the large temperature variation.

Core and block sampling demonstrated that the majority of the sand in the cubic test cell was well-cemented. The unconfined compressive strengths of three well-cemented core samples were 3.6 MPa, 4.4 MPa, and 7.6 MPa, with average $CaCO_3$ contents of 13.6 %, 15.3 %, and 14.1 %, respectively. Consolidated-drained triaxial tests on eleven sub-cored specimens also demonstrated rock-like responses of the bio-cemented sands. The peak deviatoric stresses for all specimens ranged from 3.3 MPa to 5.9 MPa under three different confining stresses (100, 300, or 500 kPa). Higher confining stress contributed to higher peak deviatoric stress, higher ultimate stress, and lower dilation. When compared with the untreated sand, which exhibits peak and ultimate fictional angles of 42.3° and 40.7° respectively, the MICP-treated sand showed enhanced peak and ultimate frictional angles of 43.6° and 42.0°, respectively. The peak and ultimate cohesions of the MICP-treated sand were determined to be 0.64 MPa and 0.12 MPa, respectively.

P-wave velocity, peak and ultimate strengths, and secant modulus of the tested bio-cemented specimens exhibited no correlation with $CaCO_3$ content. P-wave velocity was influenced by large spatial variations in the initial grain size distribution and grain shape, visualised using X-CT images, alongside variations in the initial dry density. Our study shows that in these highly heterogeneous sand deposits, absolute values of P-wave velocity would not be sufficient to assess the level of soil improvement achieved as a result of MICP treatment, but rather as a minimum P-wave velocity monitoring should involve taking readings prior to, and after, MICP treatment.

CRediT authorship contribution statement

Guijie Sang: Writing – original draft, Visualization, Methodology, Investigation, Formal analysis, Data curation, Conceptualization. **Rebecca J. Lunn:** Writing – review & editing, Validation, Supervision, Resources, Project administration, Methodology, Investigation, Funding acquisition, Conceptualization. **Grainne El Mountassir:** Writing – review & editing, Validation, Supervision, Methodology, Investigation, Conceptualization. **James M. Minto:** Writing – review & editing, Validation, Methodology, Investigation, Conceptualization. **Erica McLachlan:** Project administration, Methodology, Investigation, Conceptualization. **David Bradley:** Project administration, Methodology, Investigation, Funding acquisition, Conceptualization. **Kenneth Henderson:** Project administration, Methodology, Investigation, Funding acquisition, Conceptualization.

Declaration of competing interest

The authors declare that they have no known competing financial interests or personal relationships that could have appeared to influence the work reported in this paper.

Acknowledgements

This research was funded by the BAM Nuttall/Royal Academy of Engineering Research Chair in *Biomineral Technologies for Ground Engineering*. The contribution of El Mountassir was supported by a UKRI Future Leaders Fellowship (MR/V025376/1). The authors would like to thank construction engineers Scott Young, Jim Jones, and Jim Shields from BAM Ritchies for their contributions to the MICP trial and for their technical supports on this project. Dr. Gloria Castro Quintero is also acknowledged for her contribution to the setup of the P-wave velocity testing. The authors would like to acknowledge that the X-ray computed tomography (XCT) was carried out in the Advanced Materials Research Laboratory, at the University of Strathclyde.

Appendix A. Supplementary data

Supplementary data to this article can be found online at https://doi.org/10.1016/j.enggeo.2024.107791.

Data availability

All data underpinning this publication are openly available from the University of Liverpool's Research Data Catalogue at doi: 10.17638/datacat.liverpool.ac.uk/2848

References

Alshibli, K.A., Cil, M.B., 2018. Influence of particle morphology on the friction and dilatancy of sand. J. Geotech. Geoenviron. Eng. 144, 04017118. https://doi.org/10.1061/(ASCE)GT.1943-5606.0001841.

ASTM, 2014. Standard Test Method for Rapid Determination of Carbonate Content of Soils. ASTM D4373-14, West Conshohocken, PA.

Cardoso, R., Vieira, J., Borges, I., 2023. On the use of biocementation to treat collapsible soils. Eng. Geol. 313, 106971. https://doi.org/10.1016/J.ENGGEO.2022.106971.

Chen, L., Song, Y., Fang, H., Feng, Q., Lai, C., Song, X., 2022. Systematic optimization of a novel, cost-effective fermentation medium of Sporosarcina pasteurii for microbially induced calcite precipitation (MICP). Construct. Build Mater. 348, 128632. https://doi.org/10.1016/J.CONBUILDMAT.2022.128632.

Cheng, Y.J., Tang, C.S., Pan, X.H., Liu, B., Xie, Y.H., Cheng, Q., Shi, B., 2021. Application of microbial induced carbonate precipitation for loess surface erosion control. Eng. Geol. 294, 106387. https://doi.org/10.1016/J.ENGGEO.2021.106387.

Clough, G.W., Sitar, N., Bachus, R.C., Rad, N.S., 1981. Cemented sands under static loading. J. Geotech. Eng. Div. 107, 799–817.
Darby, K.M., Hernandez, G.L., DeJong, J.T., Boulanger, R.W., Gomez, M.G., Wilson, D. W., 2019. Centrifuge model testing of liquefaction mitigation via microbially induced calcite precipitation. J. Geotech. Geoenvironmental Eng. 145, 04019084. https://doi.org/10.1061/(ASCE)GT.1943-5606.0002122.
Dejong, J.T., Soga, K., Kavazanjian, E., Burns, S., Van Paassen, L.A., Al Qabany, A., Aydilek, A., Bang, S.S., Burbank, M., Caslake, L.F., Chen, C.Y., Cheng, X., Chu, J., Ciurli, S., Esnault-Filet, A., Fauriel, S., Hamdan, N., Hata, T., Inagaki, Y., Jefferis, S., Kuo, M., Laloui, L., Larrahondo, J., Manning, D.A.C., Martinez, B., Montoya, B.M., Nelson, D.C., Palomino, A., Renforth, P., Santamarina, J.C., Seagren, E.A., Tanyu, B., Tsesarsky, M., Weaver, T., 2013. Biogeochemical processes and geotechnical applications: Progress, opportunities and challenges. Bio- Chemo- Mech. Process. Geotech. Eng. - Geotech. Symp. Print 2013, 143–157. https://doi.org/10.1680/bcmpge.60531.014.
DeJong, J.T., Gomez, M.G., San Pablo, A.C., Graddy, C.M.R., Nelson, D.C., Lee, M., Ziotopoulou, K., El Kortbawi, M., Montoya, B., Kwon, T.H., 2022. State of the Art: MICP soil improvement and its application to liquefaction hazard mitigation. In: Proc. 20th ICSMGE-State Art Invit. Lect.
El Mountassir, G., Minto, J.M., van Paassen, L.A., Salifu, E., Lunn, R.J., 2018. Applications of Microbial Processes in Geotechnical Engineering. Adv. Appl. Microbiol. 104, 39–91. https://doi.org/10.1016/BS.AAMBS.2018.05.001.
Feng, K., Montoya, B.M., 2016. Influence of confinement and cementation level on the behavior of microbial-induced calcite precipitated sands under monotonic drained loading. J. Geotech. Geoenvironmental Eng. 142, 04015057. https://doi.org/10.1061/(ASCE)GT.1943-5606.0001379.
Gomez, M.G., Martinez, B.C., DeJong, J.T., Hunt, C.E., deVlaming, L.A., Major, D.W., Dworatzek, S.M., 2015. Field-scale bio-cementation tests to improve sands. Proc. Inst. Civ. Eng. - Gr. Improv. 168, 206–216. https://doi.org/10.1680/grim.13.00052.
Gomez, M.G., Anderson, C.M., Graddy, C.M.R., DeJong, J.T., Nelson, D.C., Ginn, T.R., 2017. Large-Scale Comparison of Bioaugmentation and Biostimulation Approaches for Biocementation of Sands. J. Geotech. Geoenvironmental Eng. 143, 04016124. https://doi.org/10.1061/(ASCE)GT.1943-5606.0001640.
Ismail, M.A., Joer, H.A., Randolph, M.F., Meritt, A., 2002. Cementation of porous materials using calcite. Geotechnique 52, 313–324. https://doi.org/10.1680/geot.2002.52.5.313.
Kwak, E., Kim, J.H., Choi, J.W., Lee, S., 2023. Injection strategy for effective bacterial delivery in bioaugmentation scheme by controlling ionic strength and pore-water velocity. J. Environ. Manage. 328, 116971. https://doi.org/10.1016/J.JENVMAN.2022.116971.
Lee, M., Gomez, M.G., Graddy, C.M.R., San Pablo, A.C.M., DeJong, J.T., Nelson, D.C., 2023. Improving the spatial control of soil biocementation using indigenous microorganisms: Column experiments and reactive transport modeling. Eng. Geol. 318, 107104. https://doi.org/10.1016/J.ENGGEO.2023.107104.
Liu, B., Zhu, C., Tang, C.S., Xie, Y.H., Yin, L.Y., Cheng, Q., Shi, B., 2020. Bio-remediation of desiccation cracking in clayey soils through microbially induced calcite precipitation (MICP). Eng. Geol. 264, 105389. https://doi.org/10.1016/J.ENGGEO.2019.105389.
Liu, B., Xie, Y.H., Tang, C.S., Pan, X.H., Jiang, N.J., Singh, D.N., Cheng, Y.J., Shi, B., 2021. Bio-mediated method for improving surface erosion resistance of clayey soils. Eng. Geol. 293, 106295. https://doi.org/10.1016/J.ENGGEO.2021.106295.
Ma, G., He, X., Jiang, X., Liu, H., Chu, J., Xiao, Y., 2021. Strength and permeability of bentonite-assisted biocemented coarse sand. Can. Geotech. J. 58, 969–981. https://doi.org/10.1139/CGJ-2020-0045/ASSET/IMAGES/CGJ-2020-0045EQ7.GIF.
Ma, G., Xiao, Y., He, X., Li, J., Chu, J., Liu, H., 2022. Kaolin-nucleation-based biotreated calcareous sand through unsaturated percolation method. Acta Geotech. 17, 3181–3193. https://doi.org/10.1007/S11440-022-01459-Y/FIGURES/12.
Miao, L., Wang, H., Sun, X., Wu, L., Fan, G., 2024. Effect analysis of biomineralization for solidifying desert sands. Biogeotechnics 2, 100065.
Minto, J.M., MacLachlan, E., El Mountassir, G., Lunn, R.J., 2016. Rock fracture grouting with microbially induced carbonate precipitation. Water Resour. Res. 52, 8827–8844. https://doi.org/10.1002/2016WR018884.
Montoya, B.M., Dejong, J.T., 2013. Healing of biologically induced cemented sands. Geotech. Lett. 3, 147–151. https://doi.org/10.1680/GEOLETT.13.00044/ASSET/IMAGES/SMALL/GEOLETT3-147-F3.GIF.
Montoya, B.M., Dejong, J.T., Boulanger, R.W., 2013. Dynamic response of liquefiable sand improved by microbial-induced calcite precipitation. Bio- Chemo- Mech. Process. Geotech. Eng. - Geotech. Symp. Print 2013, 125–135. https://doi.org/10.1680/BCMPGE.60531.012.
Nafisi, A., Asce, S.M., Montoya, B.M., Asce, M., Evans, T.M., Asce, A.M., 2020. Shear Strength Envelopes of Biocemented Sands with varying Particle size and Cementation Level. J. Geotech. Geoenvironmental Eng. 146, 04020002. https://doi.org/10.1061/(ASCE)GT.1943-5606.0002201.
Omoregie, A.I., Khoshdelnezamiha, G., Senian, N., Ong, D.E.L., Nissom, P.M., 2017. Experimental optimisation of various cultural conditions on urease activity for isolated Sporosarcina pasteurii strains and evaluation of their biocement potentials. Ecol. Eng. 109, 65–75. https://doi.org/10.1016/J.ECOLENG.2017.09.012.
Omoregie, A.I., Palombo, E.A., Ong, D.E.L., Nissom, P.M., 2020. A feasible scale-up production of Sporosarcina pasteurii using custom-built stirred tank reactor for in-situ soil biocementation. Biocatal. Agric. Biotechnol. 24, 101544.
Rodríguez, R., Cardoso, R., 2024. Applicability of electrical resistivity measurements for monitoring biocementation treatment in soils. Eng. Geol. 335, 107533. https://doi.org/10.1016/J.ENGGEO.2024.107533.
Salifu, E., MacLachlan, E., Iyer, K.R., Knapp, C.W., Tarantino, A., 2016. Application of microbially induced calcite precipitation in erosion mitigation and stabilisation of sandy soil foreshore slopes: a preliminary investigation. Eng. Geol. 201, 96–105. https://doi.org/10.1016/J.ENGGEO.2015.12.027.
San Pablo, A.C.M., DeJong, J.T., Carey, T.J., 2024. Influence of biocementation treatment extent on dynamic system performance: a centrifuge liquefaction study. Soil Dyn. Earthq. Eng. 183, 108792. https://doi.org/10.1016/J.SOILDYN.2024.108792.
Sang, G., Lunn, R.J., El Mountassir, G., Minto, J.M., 2023a. Transport and Fate of Ureolytic Sporosarcina pasteurii in Saturated Sand Columns: experiments and Modelling. Transp. Porous Media 149, 599–624. https://doi.org/10.1007/s11242-023-01973-x.
Sang, G., Lunn, R.J., El Mountassir, G., Minto, J.M., 2023b. Meter-scale MICP improvement of medium graded very gravelly sands: lab measurement, transport modelling, mechanical and microstructural analysis. Eng. Geol. 324, 107275. https://doi.org/10.1016/j.enggeo.2023.107275.
Sharma, M., Satyam, N., Reddy, K.R., 2022. Large-scale spatial characterization and liquefaction resistance of sand by hybrid bacteria induced biocementation. Eng. Geol. 302, 106635. https://doi.org/10.1016/j.enggeo.2022.106635.
Skempton, A.W., 1954. The pore-pressure coefficients A and B. Geotechnique 4, 143–147. https://doi.org/10.1680/GEOT.1954.4.4.143.
Steinacher, F., 2021. The Potential for Microbially Induced Carbonate Precipitation to Support Wellbore Sealing and Zonal Isolation in the Hydrocarbon Industry. University of Strathclyde, Glasgow.
van Paassen, L.A., 2011. Bio-mediated ground improvement: from laboratory experiment to pilot applications. Proceeding Geo-Frontiers; Adv. Geotech. Eng. 4099–4108.
van Paassen, L.A., Ghose, R., van der Linden, T.J.M., van der Star, W.R.L., van Loosdrecht, M.C.M., 2010. Quantifying Biomediated Ground Improvement by Ureolysis: Large-Scale Biogrout Experiment. J. Geotech. Geoenvironmental Eng. 136, 1721–1728. https://doi.org/10.1061/(ASCE)GT.1943-5606.0000382.
Weil, M.H., DeJong, J.T., Martinez, B.C., Mortensen, B.M., 2012. Seismic and resistivity measurements for real-time monitoring of microbially induced calcite precipitation in sand. Geotech. Test. J. 35, 330–341.
Whiffin, V.S., 2004. Microbial CaCO3 Precipitation for the Production of Biocement. PhD Thesis. Murdoch University, Western Australia.
World Weather Online, 2022. Historical Weather (from 31-05-2022 to 23-06-2022) at Kilsyth, North Lanarkshire, GB [WWW Document]. URL. https://www.worldweatheronline.com/kilsyth-weather-history/north-lanarkshire/gb.aspx.
Wu, S., Li, B., Chu, J., 2021. Stress-Dilatancy Behavior of MICP-Treated Sand. Int. J. Geomech. 21, 04020264. https://doi.org/10.1061/(ASCE)GM.1943-5622.0001923.
Wu, H., Wu, W., Liang, W., Dai, F., Liu, H., Xiao, Y., 2023. 3D DEM modeling of biocemented sand with fines as cementing agents. Int. J. Numer. Anal. Methods Geomech. 47, 212–240. https://doi.org/10.1002/NAG.3466.
Xiao, Y., Ma, G., Wu, H., Lu, H., Zaman, M., 2022. Rainfall-Induced Erosion of Biocemented Graded Slopes. Int. J. Geomech. 22, 04021256. https://doi.org/10.1061/(ASCE)GM.1943-5622.0002239/ASSET/ABF6AD87-28CC-4891-925A-5BA7A08E27D7/ASSETS/IMAGES/LARGE/FIGURE9.JPG.
Zamani, A., Montoya, B.M., Gabr, M.A., 2019. Investigating challenges of in situ delivery of microbial-induced calcium carbonate precipitation (MICP) in fine-grain sands and silty sand. Can. Geotech. J. 56, 1889–1900.
Zeng, C., Veenis, Y., Hall, C.A., Young, E.S., van der Star, W.R.L., Zheng, J., van Paassen, L.A., 2021. Experimental and Numerical Analysis of a Field Trial Application of Microbially Induced Calcite Precipitation for Ground Stabilization. J. Geotech. Geoenvironmental Eng. 147, 05021003. https://doi.org/10.1061/(ASCE)GT.1943-5606.0002545.
Zhang, A., Dieudonné, A.-C., 2023. Effects of carbonate distribution pattern on the mechanical behaviour of bio-cemented sands: a DEM study. Comput. Geotech. 154, 105152.
Zhang, X., Chen, Y., Liu, H., Zhang, Z., Ding, X., 2020. Performance evaluation of a MICP-treated calcareous sandy foundation using shake table tests. Soil Dyn. Earthq. Eng. 129, 105959. https://doi.org/10.1016/J.SOILDYN.2019.105959.